Supporting Information

Single-stranded DNA designed lipophilic G-quadruplex as transmembrane channels for switchable potassium transport

Chunying Li, Hui Chen, Li Zhou, Hui Shi, Xiaoxiao He, Xiaohai Yang,* Kemin Wang, Jianbo Liu*

State Key Laboratory of Chemo/Biosensing and Chemometrics, College of Chemistry and Chemical Engineering, Key Laboratory for Bio-Nanotechnology and Molecular Engineering of Hunan Province, Hunan University, Changsha 410082, P. R. China.

Tel/Fax: +86-731-8882-3930, E-mail: liujianbo@hnu.edu.cn, yangxiaohai@hnu.edu.cn.

Contents

Experimental Procedures

S1. Materials and reagents

S2. Instrumentation and characterisation

S3. Design of G-quadruplex ssDNA

S4. Preparation of DPPC large unilamellar vesicles (LUVs)

S5. HPTS ion transport assays

S6. Safranin O fluorescence assays

S7. Preparation of giant unilamellar vesicles (GUV) for confocal imaging

S8. Ion currents measurement

S9. Switchable ion transport experiments

Figures

Fig. S1. The structure of the linker, of FAM and how FAM, cholesterol, and spacers are connected to the nucleotides.

Fig. S2. ESI-MS of Oligonucleotide ssDNA sequences

Fig. S3. ESI-MS, ABTS catalysis for lipoG4

Fig. S4. CD spectra,ESI-MS, ABTS catalysis and GUV imaging for G4

Fig. S5. TEM image, hydrodynamic size, and zeta potential of LUV

Fig. S6. HPTS fluorescent assays with lipoG4 and G4

Fig. S7. The fitting curve for the initial rates

Fig. S8. Variable temperature HPTS assays

Fig. S9. Gaussian fit for planer lipid bilayer single-channel conductance

Fig. S10. Ion-triggered switch response of lipoG4 and CD spectra

Fig. S11. HPTS assays and switchable transport in response of Cd^{2+}/L-Cys

Experimental Procedures

S1. Materials and reagents

1,2-dioleoyl-sn-glycero-3-phosphocholine (DOPC, 99%), 1,2 dipalmitoyl- sn-glycero-3-phosphocholine(DPPC, 99%), L-α-phosphatidylcholine (EYPC, 99%), Oleic acid (90%), cholesterol (99.5%), 2,2'-azino-bis(3-ethylthiazoline-6-sulfonic acid) (ABTS, 98.0%), 8-hydroxyindole-1,3,6-trisulphonic acid trisodium (HPTS, 87%) and L-cysteine (L-Cys, 98%) were obtained from Sigma Aldrich. 3,7-diamino-5- phenylphenazinium chloride (Safranin O, 95.5%) was purchased from Belling. Gramicidin A was obtained from Enzo. Potassium tripolyphosphate ($K_5P_3O_{10}$, 95%) and anhydrous dysprosium (III) chloride ($DyCl_3$, 99.9%) were purchased from Macklin. Barium chloride ($BaCl_2$, 99%), magnesium chloride ($MgCl_2$, 98%), zinc chloride ($ZnCl_2$, 98%) and N-methyl mesoporphyrin IX (NMM, 98%) were purchased from J&K Scientific. All the oligonucleotide sequences, including lipoG4, G4, FAM-lipoG4, FAM-G4 were purchased from Sangon Biotech (Shanghai, China). DNA synthesis was performed by solid phase phosphonamidite method, purified by high performance liquid chromatography (HPLC), and analysed by mass spectrometry (LC-MASS).

S2. Instrumentation and characterisation

UV/Vis adsorption measurements were conducted using a Shimadzu UV/vis 1601 spectrophotometer at 25 °C. Fluorescent emission spectra and time-dependent fluorescence scanning were performed using a Hitachi F-7000 fluorescence spectrophotometer. Circular dichroism (CD) spectra were generated using a MOS-500 spectropolarimeter at 230–340 nm. Zeta potential and dynamic light scattering measurements were performed using a Malvern Zetasizer Nano-ZS instrument equipped with a 633-nm laser. Samples were injected into a disposable zeta cuvette at 25 °C with a scattering angle of 175°. Electrospray ionisation-mass spectroscopy (ESI-MS) was performed at Thermo Scientific Orbitrap Elite.

S3. Design of G-quadruplex ssDNA.

LipoG4 and G4 sequences were synthesized using a standard automated DNA synthesis protocol. Gradual introduction of K^+ ions (0–10 mM) into the lipoG4 or G4 ssDNA sequences (2.0 μM) led to the formation of G-quadruplex structure. G-quadruplex structures were verified in circular dichroism, and Electrospray ionization mass spectrometers. Peroxidase-like catalysis activity of G-quadruplex-hemin complex was charaterized through conversion of ABTS into the $ABTS^{\cdot+}$ radical (adsorption peak at 420 nm) in the presence of H_2O_2.

S4. Preparation of DPPC large unilamellar vesicles (LUVs)

DPPC LUVs were prepared using a lipid film hydration method. In typical procedures, DPPC lipids (30 μM) and cholesterol (5.1 μM) were incubated in chloroform (1.0 mL) for

5 min at room temperature. The chloroform was then removed using a rotary evaporator and the resulting thin films were kept *in vacuo* for 5 h at 0 °C prior to adding 1 mL aliquots of HEPES buffer (20 mM; pH 7.0) containing 100 mM KCl. Suspensions were stirred for 1 h and were then subjected to eight freeze-thaw (liq. N_2 and 40 °C) cycles. After sonicating in a bath sonicator at 15 °C for 10 min, LUVs stock suspensions containing 30 mM DPPC and 100 mM KCl were purified using an ultra-filtration centrifuge and were then stored at 4 °C in a refrigerator. For HPTS assays, 1 mL aliquots of HEPES buffer (20 mM, pH 7.0) containing 100 mM KCl and 0.5 mM HPTS dye were added, resulting in the formation of HPTS LUVs stock suspensions containing 30 mM DPPC, 100 mM KCl and 0.5 mM HPTS.

S5. HPTS ion transport assays.

DPPC LUVs were prepared using a lipid film hydration method. LUVs stock solution was diluted in 200 μL of HEPES buffer containing 2.25 mM DPPC in a cuvette. Appropriate volumes of lipoG4 or G4 ion carrier (0–3.0 μM) were then added to the cuvette and the solution was allowed to stir for 1–2 min prior to the fluorescence measurements. KOH solution (3 μL, 1 mol/L) was then added to increase the external pH by 1.0 unit and the fluorescence intensity of HPTS dye was monitored in real time at 520 nm. Finally, aqueous Triton X-100 (5%, 5 μL) was added to lyse vesicles.

After adding base pulses, rates of ion transport were determined by fitting to fluorescence curves that were obtained using Equation S1.

$$Y = AX + B \qquad \text{(Equation S1)}$$

HPTS assays were performed with various concentrations of lipoG4 or G4. Before adding detergent, fluorescence values were plotted against concentrations of ion carriers, and the resulting Hill plots were fitted to Equation S2 (the Hill equation) to calculate EC_{50} and n values as follows:

$$I = I_\infty + ((I_0-I_\infty)/(1+(c/EC_{50})^n)) \qquad \text{(Equation S2)}$$

In Equation S2, I_0 and I_∞ correspond with the fluorescent intensities in the absence and excess of ion carriers, respectively. EC_{50} values correspond with the ion carrier concentrations required to obtain half maximal fluorescence. The value n corresponds with numbers of ion carriers interacting with a single ion and is referred to as the Hill coefficient for ion carriers.

S6. Safranin O fluorescence assays

200 μL LUVs stock solutions were diluted with HEPES buffer (20 mM, pH 7.0) containing 300 mM KCl or 300 mM NaCl in a cuvette. Appropriate volumes of lipoG4 ion carrier (0.5 or 3.0 μM) were then added to the cuvettes and solutions were stirred for 1–2 min prior to fluorescence measurements. After addition of aqueous safranin O solution (final concentration 125 nM), fluorescence was monitored at excitation and emission at 522 and 581 nm, respectively.

S7. Preparation of giant unilamellar vesicles (GUV) for confocal imaging

Lipid mixtures containing EYPC (7.5 mg), DPPC (5.0 mg), cholesterol (2.0 mg) and oleic acid (1.8 mg) were dissolved in 3 mL aliquots of chloroform and added to 25 mL round-bottom flasks containing 4 mL of methanol. Solvents were removed using a rotary evaporator at 200 rpm in water at 70°C, leading to the formation of thin layers of dried phosphatide film on the walls of the round-bottom flasks. Subsequently, 10 mL aliquots of 20 mM HEPES buffer (pH 8.0) containing 300 mM KCl were carefully added to single side walls of round-bottom flasks and dry phospholipid membranes were dissolved to form GUV suspensions. FAM labelled G4 or lipoG4 (0.15 μM) was then added to 10 mL GUV suspensions. After incubation for 4 h, fluorescence staining of GUV was imaged using confocal fluorescence microscopy with a Leica F500+IX70 confocal laser scanning microscope and a 100× oil immersion objective. FAM was excited using a laser at 488 nm and emission bands were set at 535–565 nm. Images were processed using ImageJ.

S8. Ion currents measurement.

A planer lipid bilayer workstation (Warner Instruments) was used for the experiment. The currents were measured by a Warner BC-535 bilayer clamp amplifier and collected using the ML846 data acquisition system. All data was filtered at 1 kHz with 8-pole Bessel filter. A chloroform solution of DPPC/EYPC was dried under N_2 and then re-suspended in decane (25 mg/mL). The lipid solution was used to precoat and form planer lipid bilayer membrane on the 200 μm aperture of a polystyrene cup held by a chamber. The cup (*cis*, ground) and chamber (*trans*) was filled with KCl solution. Ag/AgCl electrodes were used to apply voltages and to record membrane currents. The test channel in DMSO was added to the *cis* cup and the solution was stirred for 5 min. After observation of the channel insertion, a voltage of 100 mV was applied to determine the single-channel conductance and current with time resolution of 0.2 ms.

S9. Switchable ion transport experiments.

We performed one-pot fluorescent HPTS assays to characterise switchable ion transport through in response of Cd^{2+}/L-Cys. HPTS LUVs stock solutions were diluted in 20 mM HEPES buffer (pH 7.0) containing 100 mM KCl in a cuvette to a final volume of 200 μL and a DPPC concentration of 2.5 mM. After addition of G4 or lipoG4 ion carriers at 2.0 μM, fluorescence intensities of HPTS dyes were monitored in real time at 520 nm. Subsequently, NaOH solutions (3.0 μL, 1.0 mol/L) were added as base pulse at 500 s to increase the external pH by 1.0 unit. At 980 s, 2 μL aliquots of 100 mM Cd^{2+} were added and 15 μL aliquots of 200 mM L-Cys were added at 1380 s. Finally, aqueous Triton X-100 (5%, 5 μL) was added to lyse vesicles.

Figures

A **Oligonucleotide sequences used in this work.**

Entry	Sequence (from 5' to 3')
lipoG4	C12-GGGT-C12-AGGGCGGGT-C12-TGGGA-Cholesteryl
G4	GGGTAGGGCGGGTTGGGA
FAM-lipoG4	FAM-GGGT-C12-AGGGCGGGT-C12-TGGGA-Cholesteryl
FAM-G4	FAM-GGGTAGGGCGGGTTGGGA

C12, Chol, and FAM indicated the 12-carbon, cholesterol, and FAM fluorescent dyes that conjugated to the sequences through solid phase phosphonamidite method.

B

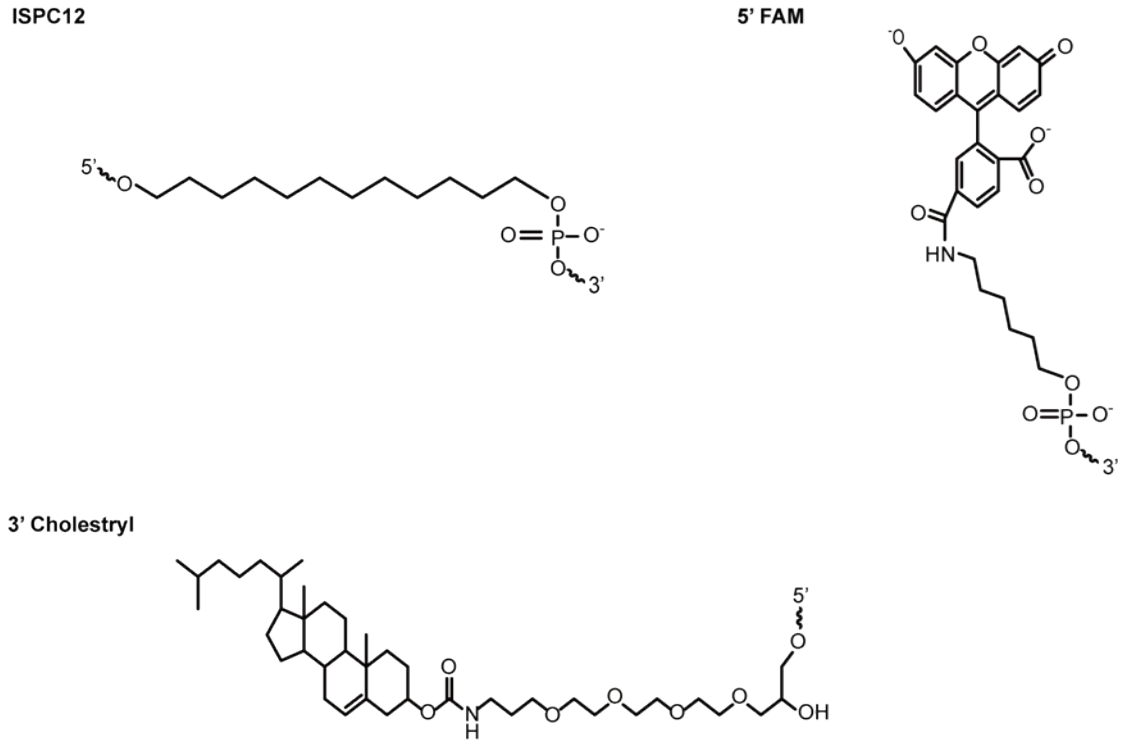

Fig. S1. Oligonucleotide sequences used in this work: lipoG4, G4, FAM-lipoG4, and FAM-G4. (A) ssDNA sequences, red highlight is lipophilic or fluorescent modification; (B) Schematic of the linker structures. ISPC12, FAM, and cholesterol are connected to the nucleotides during DNA solid phase synthesis based on the phosphoramidite method.

A

lipoG4

Calculated MW	Measured MW	Relative error (ppm)
7135.7	7133.0	0.03%

G4

Calculated MW	Measured MW	Relative error (ppm)
5717.8	5717.1	0.01%

FAM-lipoG4

Calculated MW	Measured MW	Relative error (ppm)
7409.0	7407.3	0.02%

FAM-G4

Calculated MW	Measured MW	Relative error (ppm)
6254.4	6253.9	0.01%

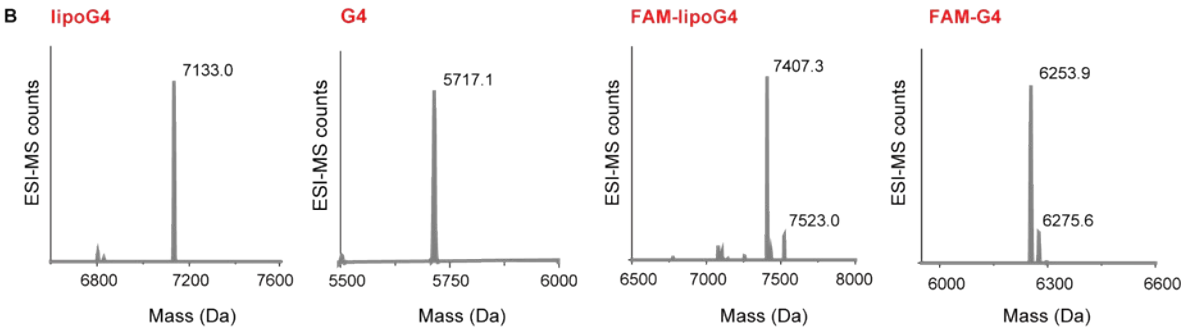

Fig. S2. (A) List of molecule weight of different DNA sequences. (B) ESI-MS for different DNA sequences. The molecular weights determined from ESI-MS were all consistent with the calculated values.

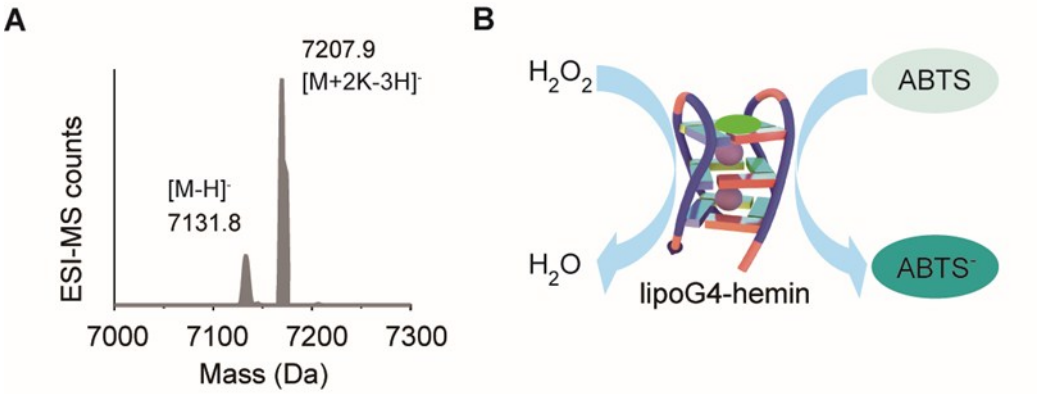

Fig. S3. (A) ESI-MS of 5 μM lipoG4 in the presence of 50 mM K^+; ESI-MS experiment in the negative-ion mode, two distinct peaks at m/z = 7131.8 and 7207.9 were determined for lipoG4. The former corresponded with the quadruplex $[M-H]^-$ and the latter corresponded with quadruplex $[M+2K-3H]^-$, which indicated the presence of two K^+ ions bound with lipoG4. (B) Schematic of the peroxidase-like catalysis activity of G-quadruplex-hemin complex and conversion of ABTS into the $ABTS^{\cdot+}$ radical (adsorption peak at 420 nm) in the presence of H_2O_2. Peroxidase-like catalysis activity could be used for confirmation of G-quadruplex formation.

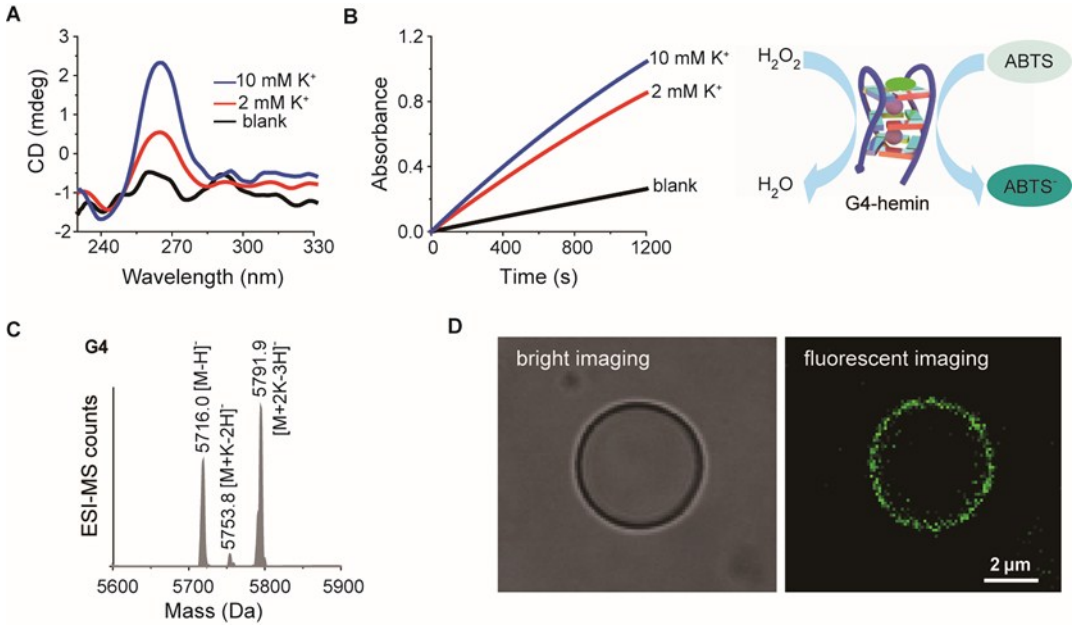

Fig. S4. (A) CD spectra of the G4 sequence in the presence of 0–10 mM K^+ ions; Gradual introduction of K^+ ions (0–10 mM) into the G4 sequences led to the appearance of a positive peak at 265 nm and a negative peak at 245 nm, indicating the formation of intramolecular G-quadruplexes with parallel conformations. (B) Time-dependent absorption changes of $ABTS^-$ radicals at 420 nm after oxidation by 2 μM G4 in the presence of 2 μM hemin, 2 μM ABTS and 500 μM H_2O_2. Gradual addition of K^+ ions facilitated the absorbance of ABTS radicals at 420 nm, indicating a peroxidation activity from lipoG4 and the formation of G-quadruplex structure. Inset: Schematic of the peroxidase-like catalysis activity of G-quadruplex-hemin complex and conversion of ABTS into the $ABTS^{\cdot+}$ radical (adsorption peak at 420 nm) in the presence of H_2O_2. Peroxidase-like catalysis activity could be used for confirmation of G-quadruplex formation. (C) ESI-MS of 5 μM G4 in the presence of 50 mM K^+; ESI-MS experiments in the negative-ion mode, two distinct peaks at m/z = 5716.0 and 5791.9 were determined for G4. The former corresponded with the quadruplex $[M-H]^-$ and the latter corresponded with quadruplex $[M+2K-3H]^-$, which indicated the presence of two K^+ ions bound with G4. (D) Bright and fluorescent image of GUV stained with FAM-G4. Ex, 488 nm; Em, 510–550 nm; scale bar, 2 μm. Low fluorescence signals were detected in phospholipid vesicles containing FAM-G4, whereas complexing mixtures of FAM-lipoG4 and GUV exhibited significant 3.7-fold increases in fluorescence around the walls of GUVs (**Fig. 1E**).

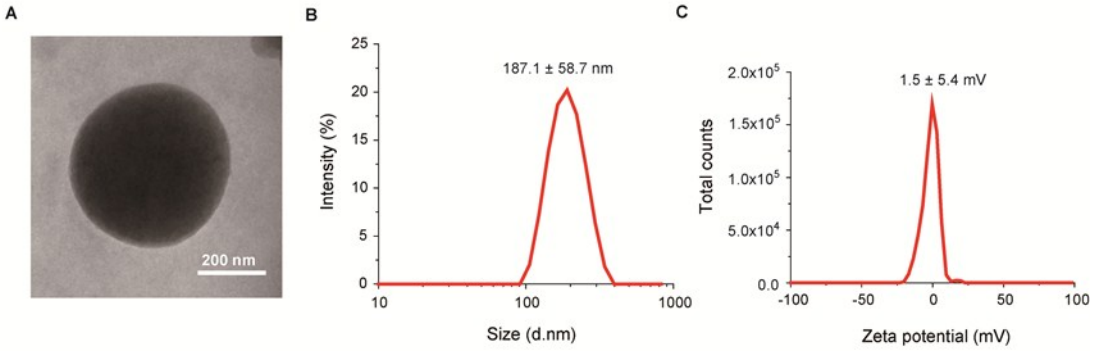

Fig. S5. TEM image (A), hydrodynamic size (B), and zeta potential (C) of LUV vesicles; hydrodynamic size and zeta potential were 187.1 ± 58.7 nm, and −1.5 ± 5.4 mV in dynamic light scattering analyses. LUV vesicles were used for HPTS transport assay.

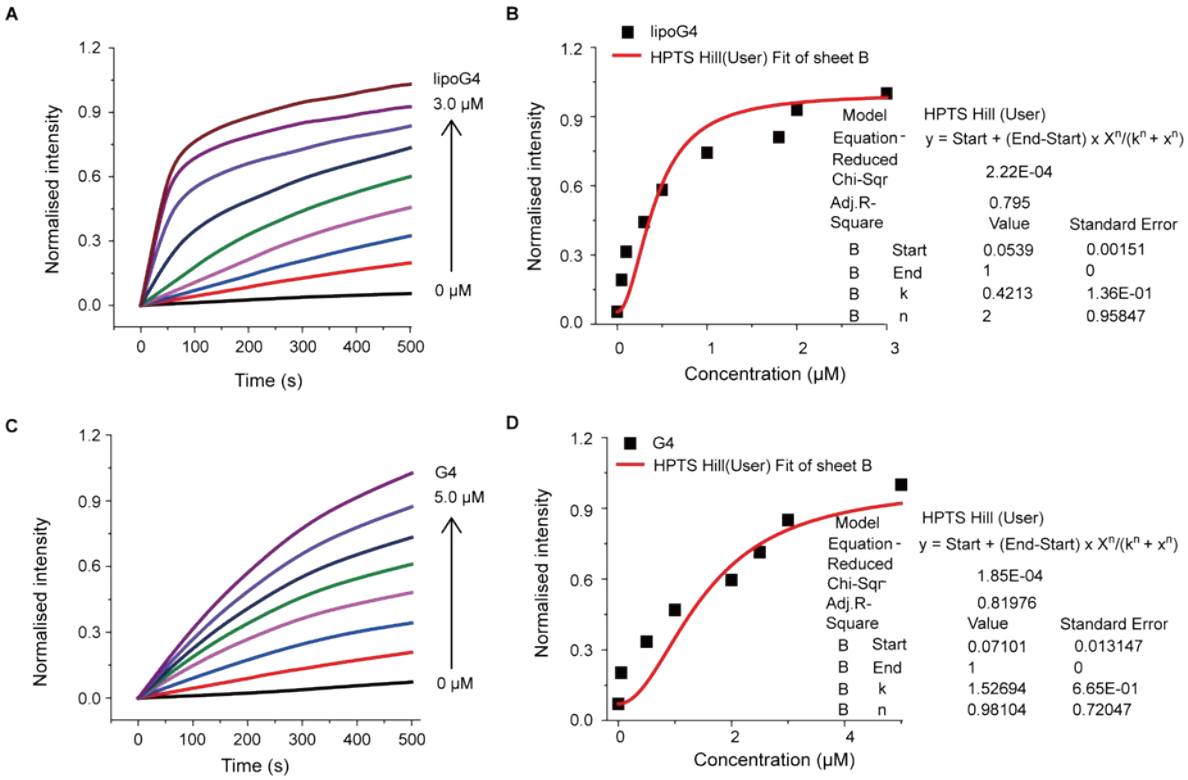

Fig. S6. HPTS fluorescent transport assays with 0-3.0 μM lipoG4 (A) and 0-5.0 μM G4 (C) In the presence of 100 mM K^+ ions, and corresponding Hill analysis fitting curves for lipoG4 (B) and G4 (D). EC_{50} values from Hill analysis were obtained to be 0.42 and 1.53 μM for lipoG4 and G4, respectively.

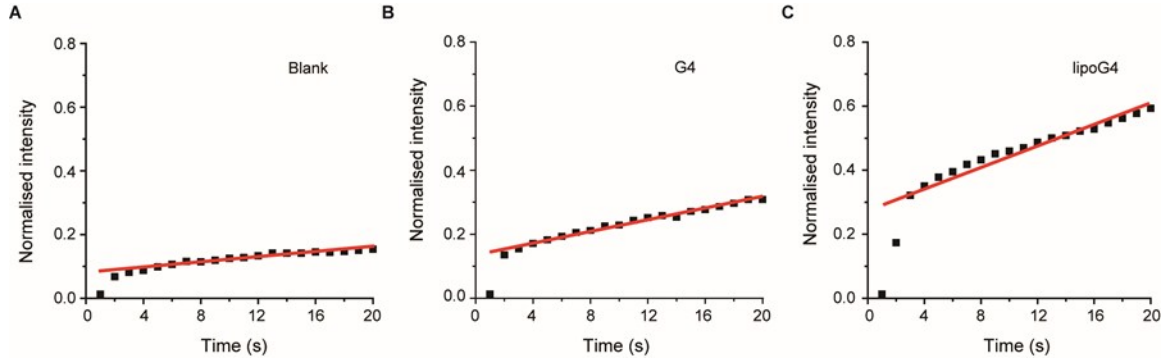

Fig. S7. Initial transport rates and fitting of the data in **Fig 2B**. Blank (A), G4 (B) and lipoG4 (C). Initial transport rates were obtained by fitting the time curves (0-20 s) to a linear equation. The rates were obtained to be: lipoG4 (k= (13.9 ± 3.9) × 10^{-3} s^{-1}), G4 (k= (7.6 ± 2.5) × 10^{-3} s^{-1}), blank (k= (2.3 ± 1.2) x 10^{-3} s^{-1}). This data was calculated in Origin 8.6 software.

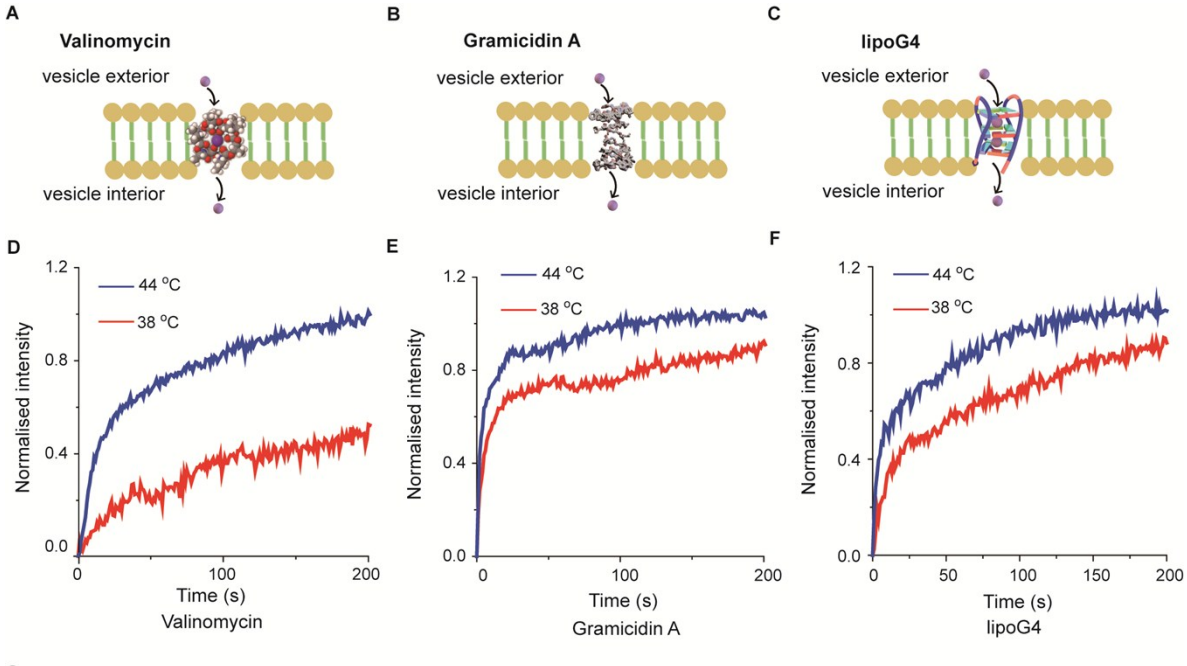

G

Initial rate (s^{-1})	Valinomycin	Gramicidin A	lipoG4
38 °C	(6.78 ± 0.54) x 10^{-3}	(22.90 ± 2.10) x 10^{-3}	(19.61 ± 1.57) x 10^{-3}
44 °C	(12.16 ± 0.24) x10^{-3}	(26.26 ± 1.49) x 10^{-3}	(25.11 ± 3.75) x 10^{-3}

Fig. S8. (A-C) Schematic of carrier and channel mechanisms investigation for ion transport; (A) valinomycin (carrier mechanism), (B) gramicidin A dimer (channel mechanism), (C) lipoG4; (D-F) Variable temperature HPTS assays with different transporters at 38 °C or 44 °C. (D) 50 μM valinomycin, (E) 50 μM gramicidin A, or (F) 3.0 μM lipoG4. (G) initial rates of ion transport calculated from HPTS assays under various temperatures. The gel–liquid crystal transition temperature for DPPC lipid is 41 °C. When the temperature

increased from 38 °C to 44 °C, the transport rate will be largely changed for carrier-based transporter, but there is less fluctuation for channel-based transporter.

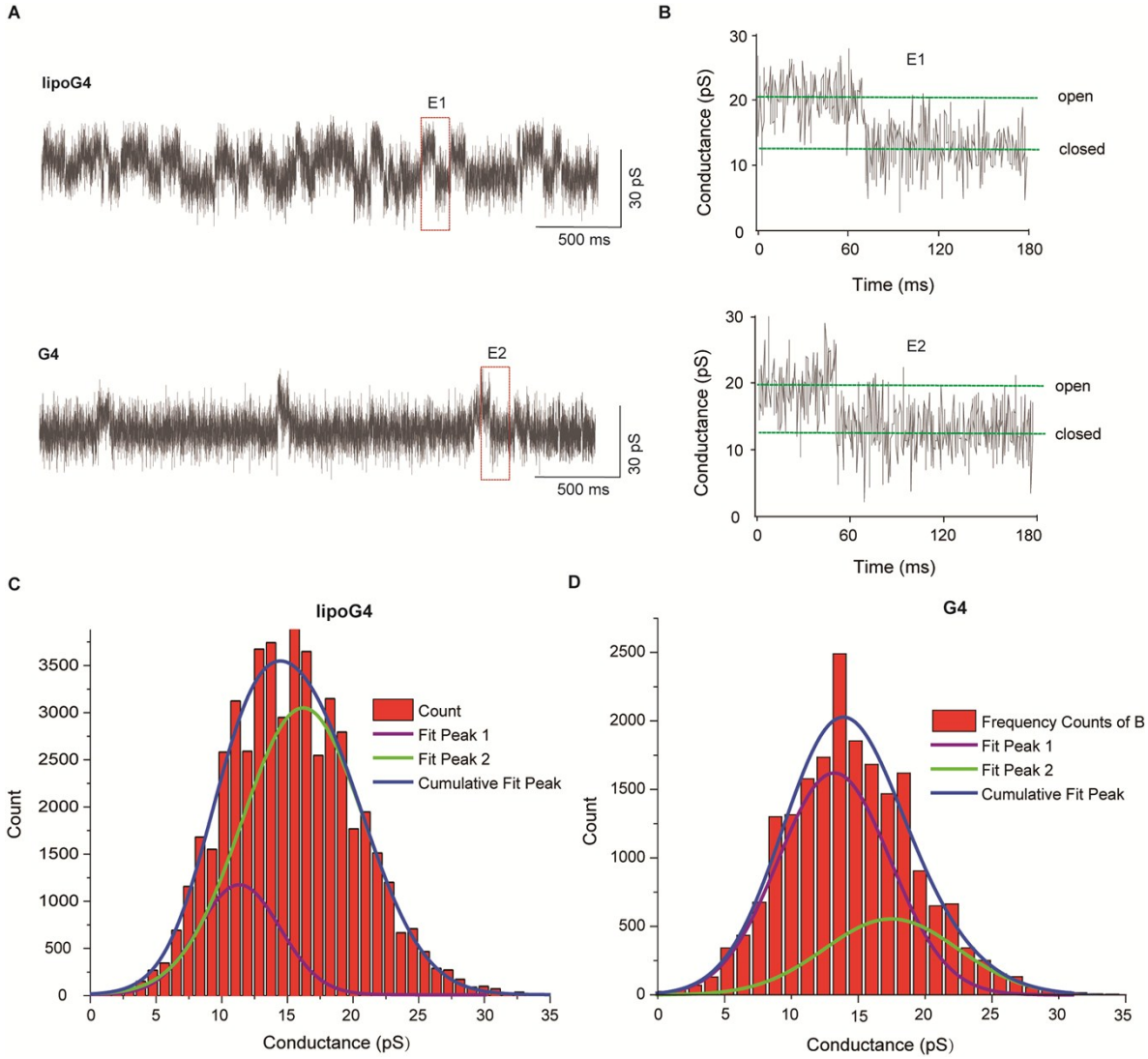

Fig. S9. (A) Planar lipid bilayer electrophysiology measurements of lipoG4 and G4 transporters at 100 mV and 1 M KCl buffer. (B) E1 and E2 are representative ionic conductance recordings of lipoG4 and G4, respectively. (C, D) Histogram with Gaussian fit for planer lipid bilayer single-channel conductance of lipoG4 (C), and G4 (D) at 100 mV. (C) The peaks were fitted through Origin 6.0 as following. $\text{peak } A1\text{: } Y_{A1} = 9.5 + \frac{9088.7}{3.1\times\sqrt{2\pi}} e^{-\frac{1}{2}\left(\frac{x-11.3}{3.1}\right)^2}$;$\text{peak } A2\text{: } Y_{A2} = 9.5 + \frac{35495.4}{4.6\times\sqrt{2\pi}} e^{-\frac{1}{2}\left(\frac{x-16.2}{4.6}\right)^2}$. The peak A1 (11.3 ± 3.1 pS) and peak A2 (16.2 ± 4.6 pS) in (A) corresponded to the close and open states, respectively, and the difference (4.9 pS) between peak A1 and peak A2 corresponded to the single-channel conductance of lipoG4. The histogram statistics of conductance also showed lipoG4 presented a probability of 79.6% in an open state (peak A2).

(D) $\text{peak } B1\text{: } Y_{B1} = -0.4 + \frac{17079.9}{4.2\times\sqrt{2\pi}} e^{-\frac{1}{2}\left(\frac{x-13.2}{4.2}\right)^2}$,

peak $B2$: $Y_{B2} = -0.4 + \frac{6940.3}{5.0\times\sqrt{2\pi}} e^{-\frac{1}{2}\left(\frac{x-17.5}{5.0}\right)^2}$. The peak B1 (13.2 ± 4.2 pS) and peak B2 (17.5 ± 5.0 pS) in (D) corresponded to the close and open states, respectively, and the difference (4.3 pS) between peak B1 and peak B2 corresponded to the single-channel conductance of G4. The histogram statistics of conductance also showed G4 presented a probability of 8.0% in an open state (peak B2).

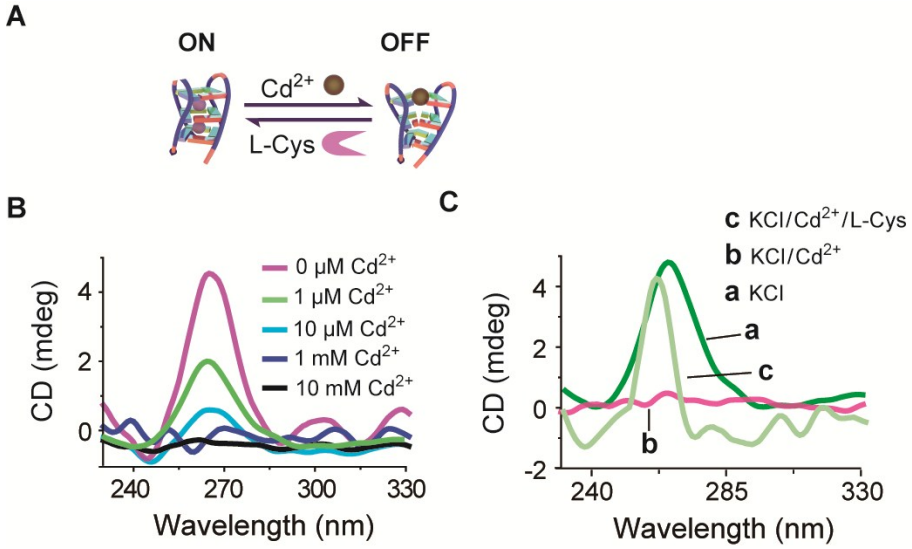

Fig. S10. (A) Illustration of lipoG4 mediated conformation transformation in response to Cd^{2+} and L-Cys. (B) CD spectra of 2 μM lipoG4 in the presence of different concentrations of Cd^{2+} ions. Cd^{2+}: 0 - 10 mM, K^{+}: 100mM. (C) CD spectra of lipoG4 in the presence of different ions. (a) 100 mM KCl; (b) 100 mM KCl, 10 mM Cd^{2+}; (c) 100 mM KCl, 10 mM Cd^{2+}, 20 mM L-Cys.

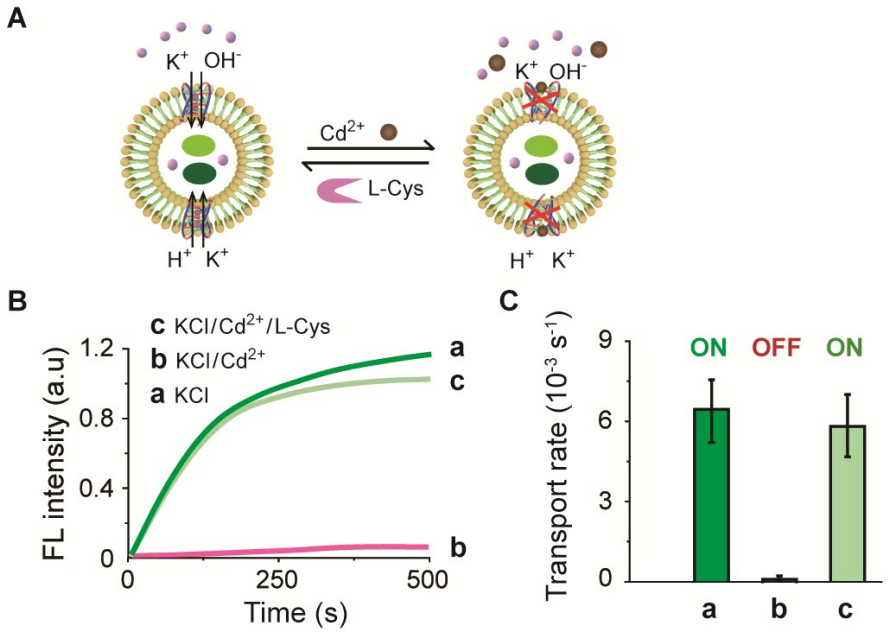

Fig. S11. (A) Schematic illustration of lipoG4 mediated transport switch in response to Cd^{2+}/L-Cys. (B) HPTS transport assay and (C) transport rate mediated by lipoG4 in the presence of different ions. (a) 100 mM KCl; (b) 100 mM KCl, 10 mM Cd^{2+}; (c) 100 mM KCl, 10 mM Cd^{2+}, 20 mM L-Cys. The HPTS assay reflected that the lipoG4 mediated transmembrane transport could be switchable controlled in response of Cd^{2+}/L-Cys.